Structure
Article

Structural Characterization of a Mouse Ortholog of Human NEIL3 with a Marked Preference for Single-Stranded DNA

Minmin Liu,[1,2] Kayo Imamura,[1,2] April M. Averill,[1] Susan S. Wallace,[1,*] and Sylvie Doublié[1,*]
[1]Department of Microbiology and Molecular Genetics, The Markey Center for Molecular Genetics, University of Vermont, Stafford Hall, 95 Carrigan Drive, Burlington, VT 05405-0068, USA
[2]These authors contributed equally to this work
*Correspondence: susan.wallace@uvm.edu (S.S.W.), sylvie.doublie@uvm.edu (S.D.)
http://dx.doi.org/10.1016/j.str.2012.12.008

SUMMARY

Endonuclease VIII-like 3 (Neil3) is a DNA glycosylase of the base excision repair pathway that protects cells from oxidative DNA damage by excising a broad spectrum of cytotoxic and mutagenic base lesions. Interestingly, Neil3 exhibits an unusual preference for DNA with single-stranded regions. Here, we report the 2.0 Å crystal structure of a Neil3 enzyme. Although the glycosylase region of mouse Neil3 (MmuNeil3Δ324) exhibits the same overall fold as that of other Fpg/Nei proteins, it presents distinct structural features. First, MmuNeil3Δ324 lacks the αF-β9/10 loop that caps the flipped-out 8-oxoG in bacterial Fpg, which is consistent with its inability to cleave 8-oxoguanine. Second, Neil3 not only lacks two of the three void-filling residues that stabilize the opposite strand, but it also harbors negatively charged residues that create an unfavorable electrostatic environment for the phosphate backbone of that strand. These structural features provide insight into the substrate specificity and marked preference of Neil3 for ssDNA.

INTRODUCTION

Nearly all organisms possess an elaborate defense system against oxidative DNA damage caused by reactive oxygen species (ROS), which are generated from normal cellular metabolism and from various exogenous sources (Duclos et al., 2012a; Wallace, 2002). The primary defense is the base excision repair pathway (BER), which is initiated by DNA glycosylases that scan the DNA and find the damaged bases. DNA glycosylases then flip the target base into their active site, cleave the N-glycosylic bond, and release the base from the sugar backbone, resulting in an apurinic or apyrimidinic (AP) site. Some of the DNA glycosylases are bifunctional and have a lyase activity that cleaves the AP site (David et al., 2007). Subsequently, a series of BER enzymes including phosphodiesterases, AP endonucleases, DNA polymerases, and ligases complete the lesion repair in several concerted steps (Hegde et al., 2008).

Based on structural and sequence homology, the DNA glycosylases specialized for oxidized base lesions fall into two families, the helix-hairpin-helix (HhH) family—represented by endonuclease III (Nth) and 8-oxoguanine DNA glycosylase (Ogg1)—and the Fpg/Nei family—represented by formamidopyrimidine DNA glycosylase (Fpg) and endonuclease VIII (Nei) in bacteria and endonuclease VIII-like 1(Neil1), Neil2, and Neil3 in mammals (Duclos et al., 2012a; Hegde et al., 2008; Wallace et al., 2003). The Fpg/Nei family members exhibit a two-domain architecture connected by a hinge region. Their N-terminal domain comprises a two-layered β sandwich structure flanked by α helices whereas their C-terminal domain comprises a bundle of α helices, two of which form a conserved helix-two-turn-helix (H2TH) motif, as well as two antiparallel β strands that form a zinc/zincless-finger motif required for DNA binding (Doublié et al., 2004; Fromme and Verdine, 2002; Gilboa et al., 2002; Imamura et al., 2009; Serre et al., 2002; Sugahara et al., 2000; Zharkov et al., 2002). The active site is located in the cleft between the two domains, with two conserved N-terminal residues (generally a proline and a glutamate) important for catalysis (Wallace et al., 2003). Members of Fpg/Nei family are equipped with a "void-filling triad" that fills the void left by the everted lesion and stabilizes the DNA helix structure (Fromme and Verdine, 2002; Kropachev et al., 2006; Zharkov et al., 2002). Fpg proteins also have an αF-β9/10 loop (located between α-helix F and β strand 9 or 10, also known as the 8-oxoG capping loop) that stabilizes 8-oxoG in the lesion-binding pocket (Fromme and Verdine, 2002; Zharkov et al., 2003). Although all Fpg/Nei family members share a similar fold, their substrate specificities are quite different. The Fpg proteins preferentially excise oxidized purines, including 8-oxo-7,8-dihydroguanine (8-oxoG) and 2,6-diamino-4-hydroxy-5-formamidopyrimidine (FapyG), whereas Nei and the Neil enzymes mainly recognize oxidized pyrimidines and adenine-derived 4,6-diamino- 5-formamidopyrimidine (FapyA) (Hegde et al., 2008; Prakash et al., 2012; Wallace et al., 2003).

Together with Neil1 and Neil2, Neil3 was identified in vertebrates as a gene product sharing significant sequence similarity with the Fpg and Nei proteins (Bandaru et al., 2002; Hazra et al., 2002a, 2002b; Morland et al., 2002; Takao et al., 2002; Wallace et al., 2003). Neil3 proteins are almost twice the size of other Fpg/Nei family members. The N terminus of the Neil3 proteins is highly conserved, with a complete Fpg/Nei-like core protein that harbors an H2TH motif and a canonical zinc finger motif.

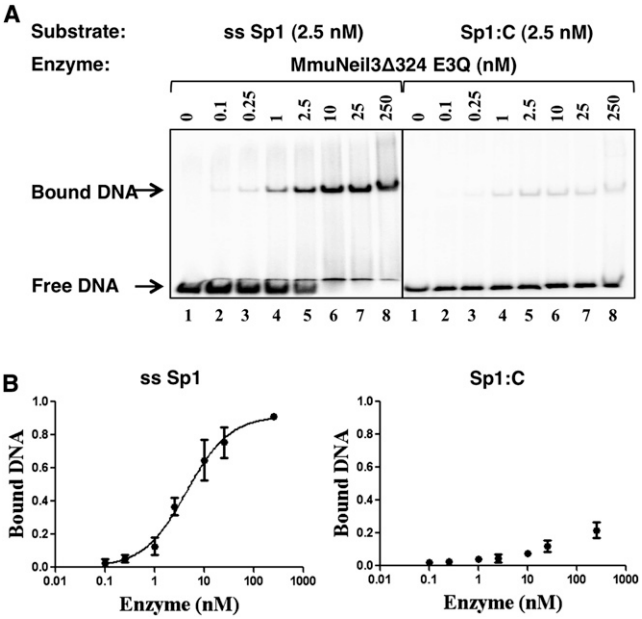

Figure 1. MmuNeil3Δ324 Preferentially Binds to ssDNA

(A) Representative gel from the EMSA of MmuNeil3Δ324 E3Q binding to 30-mer single-stranded (left) or duplex (right) substrates containing spiroiminodihydantoin (Sp1). Enzyme and substrate concentrations are as listed. (B) Quantification of the EMSA of MmuNeil3Δ324 E3Q bound to 30-mer single-stranded (left) or duplex (right) substrates containing Sp1. The fraction of the bound substrates was plotted relative to enzyme concentration. Data for single-stranded Sp1 were fit with a single hyperbola to calculate $K_D$app values. The error bars represent the standard deviation from three independent experiments.

Also see Figure S5.

Neil3 proteins also have a Ran binding protein (RanBP2)-type zinc finger motif and a duplicated GRF-zinc finger motif at their extended C terminus (Bandaru et al., 2002; Krokeide et al., 2009; Liu et al., 2010; Morland et al., 2002; Takao et al., 2009; Torisu et al., 2005). Unlike other Fpg/Nei family members, Neil3 exhibits a broad substrate recognition spectrum and can excise both oxidized purines and pyrimidines, but does not excise 8-oxoG (Liu et al., 2010). The best substrates for Neil3 are the further oxidation products of 8-oxoG, including spiroiminodihydantoin (Sp) and guanidinohydantoin (Gh), as well as FapyG and FapyA (Liu et al., 2010). Depending on the DNA sequence context, thymine glycol (Tg) can also be excised efficiently by Neil3 (J. Zhou and S.S.W., unpublished data). In γ-irradiated DNA, FapyA and FapyG are the best substrates but oxidized pyrimidines are also released (Liu et al., 2010). In DNA with single-stranded regions, the ring-saturated pyrimidines 5,6-dihydrothymine (DHT) and 5,6-dihydrouracil (DHU), and the oxidized pyrimidines 5-hydroxycytosine (5-OHC) and 5-hydroxyuracil (5-OHU) are all good substrates for Neil3 (Liu et al., 2010); in fact, Neil3 exhibits a preference for lesions in single-stranded DNA (ssDNA) as well as in bubble, fork, and quadruplex structures (Liu et al., 2010, 2012).

While several different DNA glycosylases can excise lesions from ssDNA, only a limited subset exhibit a preference for single-stranded substrates. Single-stranded selective monofunctional uracil-DNA glycosylase (SMUG1) removes uracil and 5-hydroxymethyluracil (5-hmeU) more efficiently from duplex DNA than from ss-DNA (Haushalter et al., 1999; Kavli et al., 2002; Wibley et al., 2003). The uracil-DNA glycosylases (of the same UDG superfamily as SMUG1) exhibit robust activity on duplex DNA, and their activity on ssDNA is slightly better than that on duplex DNA (Mol et al., 1995; Savva et al., 1995; Slupphaug et al., 1996; Xiao et al., 1999). Some Fpg/Nei glycosylases, such as *Escherichia coli* Fpg (EcoFpg), can recognize 8-oxoG and AP sites in both single and double-stranded DNA. However, the activity and affinity of Fpg for ssDNA is much lower than that for duplex DNA (Castaing et al., 1992; Ishchenko et al., 1999). NEIL1 can also excise lesions in bubble, bulge, and ssDNA but at a much lower rate than from duplex substrates (Dou et al., 2003; Zhao et al., 2010). In contrast, Neil3 exhibits both a faster (as much as 60 times) catalytic turnover rate and a lower K_m on ssDNA than on duplex DNA containing the same lesion (Liu et al., 2010). Of the DNA glycosylases that recognize oxidized bases, only Neil2 and Neil3 have been reported to exhibit a strong preference for single-stranded substrates (Bandaru et al., 2007; Dou et al., 2003; Hazra et al., 2002b; Liu et al., 2010, 2012). However, to date, there are no available structures of Neil2 or Neil3 proteins.

To dissect the structural features underpinning the unusual substrate specificity of Neil3, we solved the crystal structure of a mouse NEIL3 ortholog (MmuNeil3). The structure sheds light on previously undescribed glycosylase features that provide insight into the marked preference of Neil3 for ssDNA as well as its broad substrate recognition spectrum.

RESULTS

MmuNeil3Δ324 Preferentially Binds to Single-Stranded DNA

The full-length mouse Neil3 protein (MmuNeil3) consists of 606 amino acids and is substantially larger than Neil1 and Neil2. The N-terminal half of Neil3 is homologous to the bacterial Fpg/Nei proteins but its C terminus harbors additional domains such as a RanBP-like zinc finger and two GRF zinc finger motifs. Full-length mNeil3 is difficult to express in large quantities and prone to aggregation. We previously showed that a C-terminal 324-amino acid truncation variant of MmuNeil3 (MmuNeil3Δ324) is more stable than the full-length protein, can be made in milligram quantities for structural studies and, importantly, retains glycosylase activity (Liu et al., 2010).

Earlier studies indicated that MmuNeil3Δ324 has lower K_m values for single-stranded substrates relative to duplex substrates containing the same lesions, which suggested that MmuNeil3Δ324 has an intrinsic affinity for ssDNA (Liu et al., 2010). We therefore analyzed the relative affinity of MmuNeil3Δ324 for single-stranded versus double-stranded substrates containing spiroiminodihydantoin (Sp1) using gel electrophoretic mobility shift analysis (EMSA) with a variant of MmuNeil3Δ324 (E3Q) devoid of glycosylase activity. The results showed that MmuNeil3Δ324 E3Q binds to ssDNA containing Sp1 with higher affinity (with K_D app value of 4.3 ± 0.6 nM) than to the duplex substrate containing the same lesion (Figure 1). These data are consistent with our kinetics data published earlier and show that MmuNeil3Δ324 preferentially forms

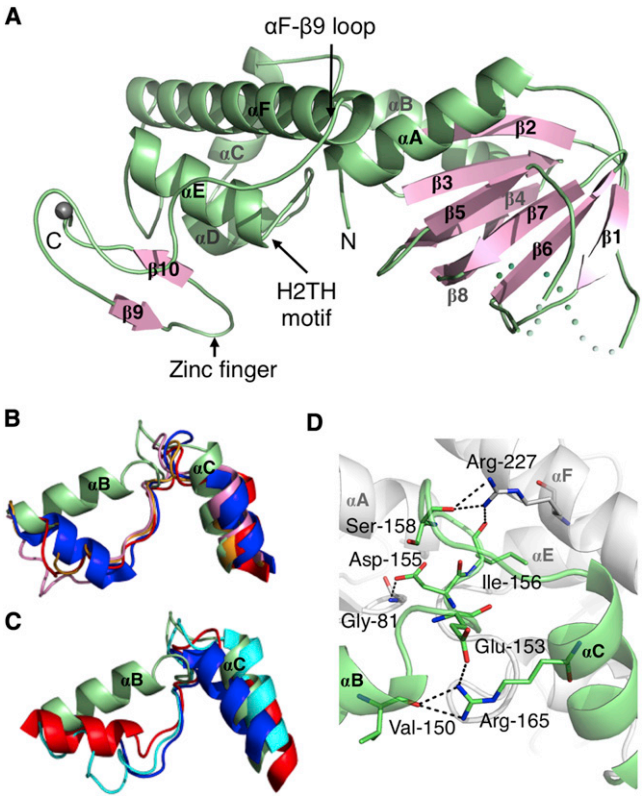

Figure 2. Overall Structure of MmuNeil3Δ324

(A) Ribbon diagram of MmuNeil3Δ324. The secondary structure elements were defined by DSSP (Kabsch and Sander, 1983) and are: αA (3–16), β1 (23–27), β2 (73–79), β3 (82–87), β4 (90–96), β5 (101–104), β6 (119–123), β7 (127–131), β8 (133–139), αB (140–150), αC (162–171), αD (177–182), αE (192–202), αF (215–238), β9 (262–264), and β10 (273–275). Helices are shown in green and β strands in pink. Residues 37–59 and 113–116 are disordered and are represented by green dots. The zinc metal ion is shown as a gray sphere.

(B) Superposition of αB-αC from MmuNeil3Δ324 (green, residues 141–172) to the corresponding segments from the Fpg proteins: *Escherichia coli* Fpg (EcoFpg, red: PDB ID code 1K82 [Gilboa et al., 2002], residues 118–147), *Thermus thermophilus* Fpg (TthFpg, pink: PDB ID code 1EE8 [Sugahara et al., 2000], residues 109–140), *Lactococcus lactis* Fpg (LlaFpg, blue: PDB ID code 1TDZ [Coste et al., 2004], residues 119–150), and *Bacillus stearothermophilus* Fpg (BstFpg, gold: PDB ID code 1R2Y [Fromme and Verdine, 2003a], residues 122–153).

(C) Superposition of αB-αC from MmuNeil3Δ324 (green) to the corresponding segments from the Nei proteins: *Escherichia coli* Nei (EcoNei, cyan: PDB ID code 1K3W [Zharkov et al., 2002], residues 113–145), NEIL1 (blue: PDB ID code 1TDH [Doublié et al., 2004], residues 126–151), and Mimivirus Nei1 (MvNei1, red: PDB ID code 3A46 [Imamura et al., 2009], residues 122–153).

(D) Close-up view of the interdomain hinge. Interacting residues are shown as stick models. Hydrogen bonds and salt bridges are represented by black dashed lines.

Also see Figure S1.

a stable complex with single-stranded substrates (Liu et al., 2010).

MmuNeil3Δ324 Exhibits an Overall Fold Similar to that of Other Fpg/Nei Family Members

To study the structural features that contribute to the unique substrate specificity of Neil3, we pursued the crystal structure of MmuNeil3Δ324, an active C-terminal deletion variant of mouse Neil3 (Liu et al., 2010, 2012). The structure of MmuNeil3Δ324 was solved by multiple isomorphous replacement at a resolution of 2.0 Å. The resulting model was refined to an R_{free} of 23.5% and R_{work} of 19.7% with good stereochemistry.

Like other Fpg/Nei family members, MmuNeil3Δ324 is a two-domain α/β protein and measures approximately 65 × 36 × 30 $Å^3$ (Figure 2A). The N-terminal domain starts with an α-helix followed by a two-layered β sandwich structure in which each layer is composed of four antiparallel β strands. The N-terminal domain ends with an α-helix and connects to the C-terminal domain via a short hinge. The C-terminal domain comprises four α helices, where αD and αE form the conserved H2TH motif, and two antiparallel β strands which form a classical zinc finger motif seen in many Fpg/Nei enzymes (Figure 2A). The overall fold of MmuNeil3Δ324 is similar to that of other Fpg/Nei family members as confirmed by the secondary structure matching (SSM) (Krissinel and Henrick, 2004) superposition results (Figure S1 available online).

Interestingly, αB in Neil3 does not overlay with the corresponding helix in the other Fpg/Nei family members, but lies perpendicular to αC (Figures 2B and 2C). The loop between αB and αC (the interdomain hinge), which connects the N- and C-terminal domain, is locked by the following interactions: Arg-165 (from αC) forms hydrogen bonds via NηH with the main-chain carbonyl group of Val-150, acting as the C-terminal cap of αB (Figure 2D). Arg-165 also forms a salt-bridge with Glu-153 in the interdomain hinge (Figure 2D). Additional stabilization comes from hydrogen bonds between the hinge loop (Asp-155, Ile-156, and Ser-158) and neighboring residues Gly-81 and Arg-227 (Figure 2D). The residues that form these interactions, namely Arg-165, Glu-153, Asp-155, and Arg-227, are highly conserved in Neil3 proteins, but not in other Fpg/Nei family members. These interactions create a more rigid segment between the N- and C-terminal domains than observed in other Fpg/Nei glycosylases and may be correlated with the preference of Neil3 for ssDNA substrates.

The Electrostatic Surface of MmuNeil3Δ324 Reveals Negative Charges along the Putative Path of the Opposite Strand

The electrostatic potential of the solvent-accessible surface residues reveals a strong positively charged cleft in Neil3 approximately orthogonal to its long axis between the N- and C-terminal domains (Figure 3A). In all Fpg/Nei family members, this cleft binds the damage-containing strand of the DNA (Figure S2). A superposition of the MmuNeil3Δ324 structure with Mimivirus Nei1 bound to DNA containing thymine glycol (Tg) (Imamura et al., 2012) shows that the Tg-containing strand fits well into the positively charged cleft in MmuNeil3Δ324 (Figure 3A). The model suggests that a flipped-out Tg inserts into an open pocket in MmuNeil3Δ324 that comprises the two catalytic residues: Val-2, which takes the place of the catalytic proline conserved in other Fpg/Nei family members (Wallace et al., 2003) and Glu-3, a residue required for glycosylase activity of Fpg/Nei enzymes (Wallace et al., 2003; Figure 3B). Superposition of MmuNeil3 with the MvNei1 structure illustrates that the N-terminal valine of Neil3 can serve the same function as the

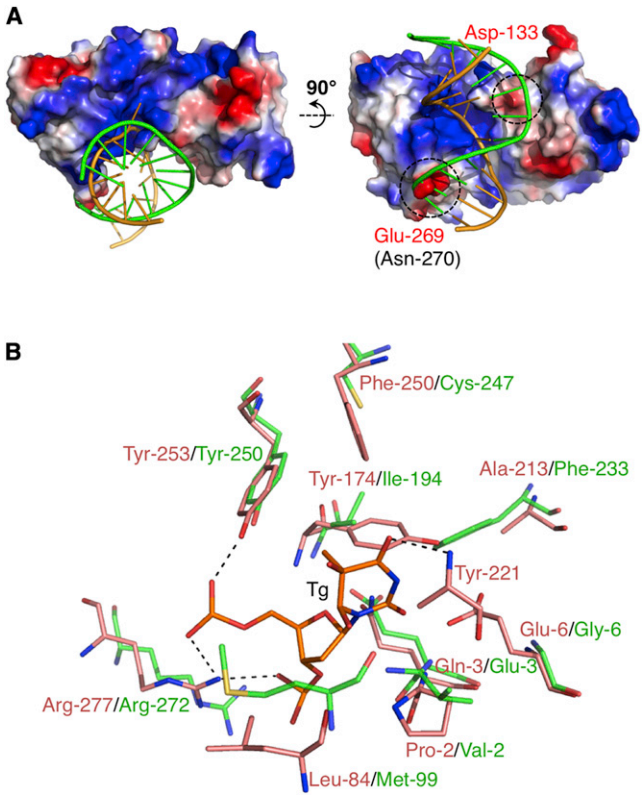

Figure 3. The DNA Binding Cleft and Lesion-Binding Pocket of MmuNeil3Δ324

(A) Electrostatic surface representation of MmuNeil3Δ324 calculated by the program GRASP (Nicholls et al., 1991), colored according to the electrostatic potential (blue, positive; red, negative). DNA from the MvNei1-Tg complex (PDB code: 3VK8; [Imamura et al., 2012]) was superimposed onto MmuNeil3Δ324. The Tg-containing strand is in orange and the complementary strand is in green.

(B) Superposition of MmuNeil3 (green) and MvNei1 in complex with Tg-containing DNA (PDB code: 3VK8 [Imamura et al., 2012]; pink) with Tg shown in gold. Hydrogen bonds between MvNei1 and Tg are represented by black dashed lines.

Also see Figure S2.

proline found in most other Fpg/Nei enzymes (Imamura et al., 2012), i.e., nucleophilic attack by the amine group of the N-terminal residue onto C1′ of the deoxyribose of the damaged base (Zharkov et al., 2002). This finding confirms our earlier observation that Val-2 in MmuNeil3 forms a Schiff base with its substrates, and that substituting Val-2 with a proline does not impede the ability of MmuNeil3 to form a Schiff base (Liu et al., 2010).

Other residues in the putative binding pocket include Met-99, a residue that fills the void created by the everted lesion in other Fpg/Nei proteins (Fromme and Verdine, 2002; Gilboa et al., 2002; Serre et al., 2002), two aromatic residues Phe-233 and Tyr-250, a hydrophobic residue Ile-194 and a glycine, Gly-6 (Figure 3B). This residue is a glutamate in all other Fpg/Nei enzymes. Although this glutamate is highly conserved, mutating it into an alanine in MvNei1 did not markedly affect its glycosylase activity (Imamura et al., 2012).

Neil3 not only lacks the basic residues that contact the phosphate backbone of the opposite strand in MvNei1 or bacterial Fpg (Figure S2), but it also harbors negatively charged residues that create an unfavorable electrostatic environment for the opposite strand (Figure S3). The acidic residues are well conserved in Neil3 proteins from all taxa and lie on both sides of the positively charged cleft along the contour of the opposite strand (Figure 3A), including Asp-133 from the β7-β8 loop, and Glu-269 at the tip of the β9-β10 loop of the zinc finger (close to the strictly conserved Arg-272, which binds the phosphate adjacent to the lesion; Fromme and Verdine, 2002; Gilboa et al., 2002; Imamura et al., 2009, 2012; Serre et al., 2002; Zharkov et al., 2002). The superposition of MmuNeil3Δ324 with the Tg-containing duplex DNA from the MvNei1-Tg complex also predicts a steric clash between Glu269/Asn270 and the opposite strand (Figure 3A). Taken together, these data indicate that the negatively charged residues along the contour of the opposite strand might destabilize the formation of a complex between Neil3 and double-stranded DNA.

Two of the "Void-Filling" Residues that Stabilize the Opposite Strand in Other Fpg/Nei Family Members Are Missing in Neil3

In addition to the electrostatic interactions with the backbone phosphate of the opposite strand, the Fpg/Nei glycosylases also utilize aromatic stacking and hydrogen-bonding to the Watson-Crick edge of the estranged base to stabilize the opposite strand. This function is fulfilled by an aromatic residue and a polar residue, which are two of the void-filling triad or intercalating residues (Banerjee et al., 2006; Coste et al., 2004; Doublié et al., 2004; Gilboa et al., 2002; Imamura et al., 2009; Zharkov et al., 2002). In EcoNei, the void-filling residues, Gln-69, Leu-70, and Tyr-71, are located in the same loop (β4-β5 loop, also known as the intercalation loop; Figure S4A) (Kropachev et al., 2006; Zharkov et al., 2002). In bacterial Fpg proteins, NEIL1 and MvNei1, one residue, generally Met or Leu, resides in the β4-β5 loop, whereas the other two residues, Phe and Arg, are found in the β7-β8 loop (Figures 4A and S4B) (Doublié et al., 2004; Fromme and Verdine, 2002; Gilboa et al., 2002; Imamura et al., 2009; Serre et al., 2002; Sugahara et al., 2000). The β4-β5 loop in Neil3 is very similar to that of the bacterial Fpg proteins, NEIL1 and MvNei1, which harbors a methionine residue to fill the void created by eversion of the lesion (Met-99; Figures 4A and S4C). In contrast, the β7-β8 loop in Neil3 is truncated, lacking four residues including two of the void-filling Phe and Arg (Figure S3). The side chain of the conserved Asp-133 is pointing outside the loop, exposing its negative charge on the surface of Neil3 (Figure 4A). Although an analogous Asp residue is found in Fpg proteins (Figure S3), in these enzymes the aspartate is buried inside the β7-β8 loop and hydrogen bonds with one or two backbone amides of the β7-β8 loop (Figure 4A).

Because of the observed differences in the β7-β8 loop between Neil3 and the Fpg proteins, we tested its potential role by creating an EcoFpg β7-β8 loop variant in which four residues at the tip of the loop (Pro108-Phe111) were mutated to four glycines. The EcoFpg β7-β8 loop variant binds to duplex DNA only when the enzyme concentration is greatly in excess over DNA, regardless of whether the oligodeoxyribonucleotide

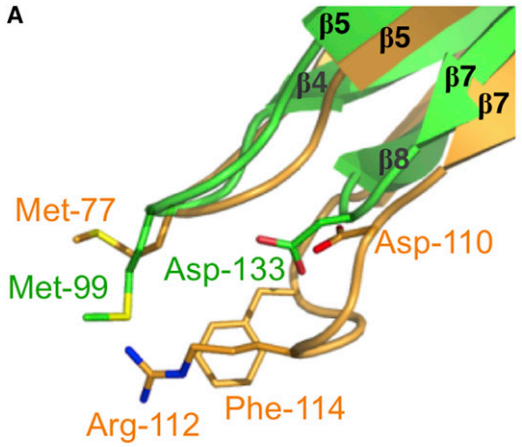

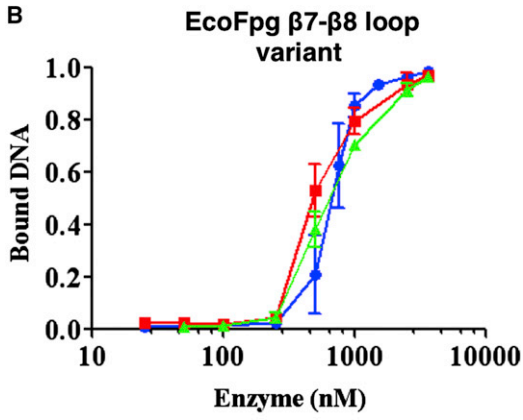

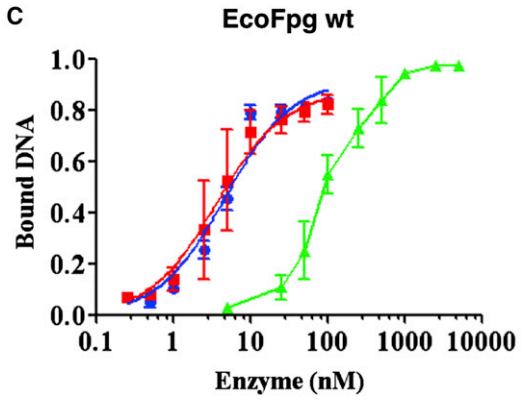

Figure 4. The Void-Filling Residues of Fpg Contribute to Binding to dsDNA

(A) Superposition of the β4-β5 and β7-β8 loops from MmuNeil3 (green) and BstFpg (gold, PDB ID code: 1R2Y [Fromme and Verdine, 2003a]). The β7-β8 loop in MmuNeil3 is shorter and lacks two of the void-filling residues.

(B) Analysis of the EMSA of the EcoFpg β7-β8 loop variant binding to duplex DNA containing THF (blue), 8-oxoG (red), or a normal base G (green).

(C) Analysis of the EMSA of wild-type EcoFpg binding to duplex DNA containing THF (blue), 8-oxoG (red), or a normal base G (green). The fraction of the bound substrates was plotted relative to enzyme concentration. Data for wild-type EcoFpg were fit with a single hyperbola to calculate $K_D$app values.

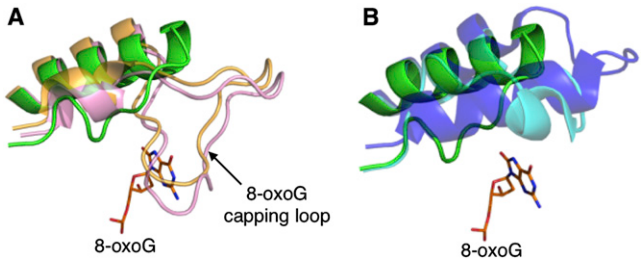

Figure 5. Close-Up View of the αF-β9 Loop of Fpg/Nei Enzymes

(A) Superposition of the αF-β9 loop from MmuNeil3Δ324 (green, residues 224–248) with BstFpg (gold, PDB ID code: 1R2Y [Fromme and Verdine, 2003a], residues 206–240) and TthFpg (pink, PDB ID code: 1EE8 [Sugahara et al., 2000], residues 193–229).

(B) with EcoNei (cyan, PDB ID code: 1Q39 [Golan et al., 2005], residues 200–228) and NEIL1 (blue, PDB ID code: 1TDH [Doublié et al., 2004], residues 228–261). The flipped-out 8-oxoG from the BstFpg-DNA complex (PDB ID code: 1R2Y [Fromme and Verdine, 2003a] is shown in orange.

Also see Figure S3.

contains a lesion (8-oxoG or tetrahydrofuran [THF]) or a normal base (G) (Figure 4B). Moreover, the enzyme-DNA complex exhibits a slow mobility band, indicating that multiple copies of the EcoFpg β7-β8 loop variant binds nonspecifically to one DNA molecule, as seen with wild-type EcoFpg bound to duplex DNA containing a normal base (Figure S5). In contrast, wild-type EcoFpg binds tightly and specifically to duplex DNA that contains a lesion, with K_D app values of 4.5 ± 0.5 nM, and 3.7 ± 0.6 nM for THF:C and 8-oxoG:C, respectively (Figure 4C). Even with the duplex DNA containing a normal base, wild-type EcoFpg exhibits tighter binding than the variant (Figures 4C and S5). These data suggest that the β7-β8 loop containing two of the void-filling residues, Phe and Arg, contributes to the specific binding of EcoFpg to duplex DNA that contains a lesion. The fact that these residues are missing in Neil3 can explain both its reduced binding affinity and catalytic turnover rate in the presence of duplex substrates.

The 8-oxoG Capping Loop Is Truncated in Neil3

A loop conserved in the bacterial Fpg proteins and located between helix αF and the zinc finger motif (the αF-β9/10 loop, also known as the 8-oxoG capping loop) wraps around and stabilizes the flipped-out 8-oxoG (Coste et al., 2004; Duclos et al., 2012b; Fromme and Verdine, 2003a). In Neil3, the corresponding loop is truncated and cannot contact a flipped-out lesion, as shown by the overlay with bacterial Fpg proteins (Figure 5A). The truncated 8-oxoG capping loop in Neil3 is also shorter than the already shortened 8-oxoG capping loop in EcoNei and NEIL1 (Figure 5B). The fact that MmuNeil3 does not recognize 8-oxoG and has a truncated αF-β9 loop is in keeping with a recent study showing that this loop has evolved to specifically recognize 8-oxoG (Duclos et al., 2012b).

The $K_D$app values of wild-type EcoFpg for THF:C and 8-oxoG:C are 4.5 ± 0.5 nM and 3.7 ± 0.6 nM, respectively. The error bars represent the standard deviation from three independent experiments.

Also see Figure S4.

DISCUSSION

Preference for DNA Containing Single-Stranded Regions

Neil3 shares many structural features with other Fpg/Nei family members, yet it harbors distinct characteristics that readily explain its preference for ssDNA: Neil3 lacks the basic residues on each side of the DNA binding cleft that interact with the phosphate backbone of the opposite strand (Figure S2). Instead, Neil3 possesses negatively charged residues (Asp-133 and Glu-269) along the contour of the opposite strand. Moreover, Glu-269 and Asn-270 at the tip of the β9-β10 loop in the zinc finger motif are predicted to sterically clash with the opposite strand. These features of Neil3 provide an explanation for its low binding affinity to the duplex substrate observed in our EMSA assays (Figure 1). NEIL2 also exhibits a preference for nonduplex substrates, such as single-stranded, fork, and bubble substrates (Dou et al., 2003; Hazra et al., 2002b). Interestingly, Neil2 proteins also possess negatively charged residues in the zinc finger motif, suggesting that these unfavorable electrostatic charges might contribute to the selection of ssDNA as well.

Importantly, Fpg/Nei glycosylases utilize two hydrophobic residues of the void-filling triad and an Arg or Gln to form hydrogen bonds to the Watson-Crick edge of the estranged bases to stabilize the opposite stand (Fromme and Verdine, 2002; Gilboa et al., 2002; Imamura et al., 2009; Serre et al., 2002; Zharkov et al., 2002). Previous studies have shown that mutating these void-filling residues resulted in substantially reduced glycosylase activity in Fpg and Nei proteins. For example, replacement of the void-filling triad with three alanine residues in EcoNei caused a 100- to 50,000-fold decrease in specificity to duplex DNA, depending on the lesion and the bases opposite the lesion (Kropachev et al., 2006). An EcoFpg variant with Phe-111 mutated to alanine showed a reduced glycosylase activity on duplex DNA containing 8-oxoG or DHU compared to the wild-type EcoFpg, which could be linked to a reduced lesion search capability (Dunn et al., 2011; Sidorenko and Zharkov, 2008). Consistent with these results, our mutational study with EcoFpg further demonstrated that the β7-β8 loop containing the void-filling triad is indispensable for the specific binding to duplex DNA (Figures 4 and S5). Therefore, the presence of the void-filling triad is a feature of the Fpg/Nei family members that contributes to their preference for lesions in duplex DNA.

The presence of the wedge residue appears to be a common feature of all other DNA glycosylases that possess robust activity on duplex DNA. In HhH glycosylases, the wedge residues insert between the base opposite the lesion and its 5′ neighbor, such as Tyr-203 in OGG1 (Bruner et al., 2000), Leu81 in *B. stearothermophilus* Nth (BstNth) (Fromme and Verdine, 2003b), Tyr-88 in *B. stearothermophilus* MutY (Fromme et al., 2004), and Leu-482 in human methyl-CpG binding domain 4 (MBD4) (Hashimoto et al., 2012; Manvilla et al., 2012). Similarly, the uracil DNA glycosylase family members, such as human UNG (Parikh et al., 1998; Slupphaug et al., 1996), *Xenopus laevis* Smug1 (Wibley et al., 2003), *E. coli* mismatch-specific uracil DNA-glycosylase (EcoMug) (Barrett et al., 1998), human thymine DNA glycosylase (TDG) (Maiti et al., 2008), all employ a conserved loop (referred to as the minor groove reading head or minor groove intercalating loop) that carries a wedge residue to intercalate into the opposite strand. Human 3-methyladenine DNA glycosylase (AAG), structurally unrelated to other DNA glycosylases, has three residues (Tyr-162, Met-164, and Tyr-165) that intercalate into the minor groove and pack against nucleotides surrounding the lesion to stabilize the DNA in a distorted conformation (Lau et al., 1998). In the structures of these DNA glycosylases, the wedge residues play an important role in stabilizing the B-form conformation of the DNA that is missing the everted lesion base. Neil3 proteins lack these wedge residues, which is consistent with their preferences for ssDNA. In summary, the preference of Neil3 for ssDNA may be due to a combination of lacking the residues necessary to stabilize duplex DNA after eversion of a base lesion and the electrostatic repulsion between negatively charged residues and the phosphate backbone of the opposite strand.

Lesion Accommodation and Recognition

Neil3 readily excises the further oxidation products of 8-oxoG, Gh, and Sp, but not 8-oxoG itself. The truncated αF-β9 loop in Neil3 explains why this protein does not cleave 8-oxoG. In the crystal structure of the BstFpg-8-oxoG complex, four consecutive main-chain amides (residues 222–225) at the tip of the αF-β9/10 loop stabilize 8-oxoG via hydrogen-bonding contacts with the exocyclic O^6, and the main-chain carbonyl of S-220 distinguishes 8-oxoG from the normal G by hydrogen-bonding with the protonated N7 of 8-oxoG (Fromme and Verdine, 2003a). The αF-β9/10 loops in bacterial Fpg proteins are similar in size and shape (Coste et al., 2004; Gilboa et al., 2002; Serre et al., 2002; Sugahara et al., 2000). Other Fpg/Nei family members with marginal activity to excise 8-oxoG, such as Nei protein from *E. coli*, NEIL1, and MvNei1, also contain an αF-β9/10 loop albeit much shorter (Figures 2 and 5) (Doublié et al., 2004; Imamura et al., 2009, 2012; Zharkov et al., 2002). A plant Fpg (AthFpg1), which has a truncated αF-β9 loop, does not have glycosylase activity on 8-oxoG-containing DNA (Duclos et al., 2012b; Kathe et al., 2009). Furthermore, truncating the αF-β9/10 loop of EcoFpg results in the loss of activity on 8-oxoG but does not affect the lyase activity or the glycosylase activity on other lesions, suggesting that the αF-β9/10 loop is specialized for stabilizing the everted 8-oxoG (Banerjee et al., 2006; Duclos et al., 2012b). Similarly Neil3 has a truncated αF-β9/10 loop and thus cannot excise 8-oxoG.

Despite the fact that MmuNeil3Δ324 exhibits low binding affinity to duplex DNA (Figure 1B), we showed earlier that it can still excise Sp and Gh from duplex DNA (Liu et al., 2010). How, then, does Neil3 recognize these lesions in duplex DNA? Sp and Gh could destabilize the DNA duplex, as evidenced by the fact that the melting temperatures of duplex DNA containing these lesions are several degrees lower than duplex DNA containing 8-oxoG or a normal base (Kornyushyna et al., 2002). Crystal structures of a DNA polymerase bound to Gh revealed that this lesion is extrahelical and rotated toward the major groove (Aller et al., 2010; Beckman et al., 2010). Molecular dynamics simulations suggested that Sp would distort the duplex by affecting base-stacking and weakening the Watson-Crick hydrogen bonding interactions in adjacent base pairs (Jia et al., 2005). Sp and Gh might cause a temporal opening of the duplex DNA, resulting in a partially

Table 1. Data Collection, Phasing, and Refinement Statistics

	Native	Gold	Platinum 1	Platinum 2
Beamlines	home source/ APS Beamline 23-ID-B	home source	home source	home source
Space group	monoclinic C2			
Unit-cell parameters (Å,°)	a = 115.58, b = 43.82, c = 77.66			
	β = 128.96			
Molecules per asymmetric unit	1			
Data Collection Statistics				
Resolution (Å)	40–2.0 (2.07–2.0)	15–2.5 (2.59–2.5)	15–2.6 (2.69–2.6)	15–2.75 (2.85–2.75)
Unique reflections	20,624 (1,976)	10,371 (1,011)	9,319 (902)	7,864 (733)
Redundancy	9.8 (3.5)	3.3	2.4	3.3
R_{merge}[a]	0.125 (0.483)	0.076 (0.230)	0.076 (0.258)	0.086 (0.151)
Completeness[a] (%)	99.7 (97.1)	99.3 (97.3)	96.4 (96.3)	98.5 (92.6)
Overall I/σ(I)[a]	16.46 (2.64)	17.3 (4.3)	12.6 (3.6)	13.9 (8.1)
MIR Phasing Statistics				
No. of sites		4	3	3
Figure of merit (SOLVE)	0.262			
Figure of merit (RESOLVE)	0.599			
Refinement Statistics				
R_{work} (%)	19.74			
R_{free} (%)	23.53			
rms deviations				
Bond length (Å)	0.0050			
Bond angles (°)	1.11			
B-factor (Å^2)				
Wilson B-factor	28.3			
Protein	30			
Water	41			
Ramachandran plot				
Most favored (%)	90.0			
Additional allowed (%)	10.0			
Generously allowed (%)	0			
Disallowed (%)	0			

$R_{merge} = \Sigma|I - \langle I\rangle|/\Sigma I$, where $\langle I\rangle$ is the average intensity from multiple observations of symmetry-related reflections. Phasing power = $\Sigma_{hkl}F_H/\Sigma|F_{PH} - F_{PH}$, calc|. R_{work} and $R_{free} = \Sigma||F_o| - |F_c||/\Sigma|F_o|$, where F_o and F_c are the observed and calculated structure factor amplitudes, respectively. R_{free} was calculated with 10% of the reflections not used in refinement. MIR, multiple isomorphous replacement.
[a]Values for the highest resolution shell are shown in parentheses.

single-stranded structure that could be recognized by the Neil3 proteins.

Implications for the In Vivo Functions of Neil3

In mice and humans, Neil3 is expressed primarily in hematopoietic tissues (Torisu et al., 2005), in tissues that harbor stem cells in the brain (Regnell et al., 2012), in various tumor tissues (Hildrestrand et al., 2009), and during embryonic development (Hildrestrand et al., 2009; Kauffmann et al., 2008; Rolseth et al., 2008; Takao et al., 2009; Torisu et al., 2005), suggesting that Neil3 function might be required in proliferating cells to remove lethal and mutagenic lesions from the genome. Moreover Neil3$^{-/-}$ mice develop profound neuropathology characterized by a reduced number of microglia and loss of proliferating neuronal progenitors in the striatum after hypoxia-ischemia (Sejersted et al., 2011). In addition, NEIL3 expressed in highly proliferative cells was found to be cell cycle-dependent and induced when cells enter S phase by mitogenic stimulation (Neurauter et al., 2012). Because Neil3 glycosylases process oxidatively induced lesions in DNA with single-stranded regions, such as fork, bubble, and quadruplex structures (Liu et al., 2010, 2012; J. Zhou and S.S.W., unpublished data), it might function during replication and in some specialized regions of the genome such as telomeres. Similarly, Neil1 and Neil2 have been proposed to function during replication and transcription, respectively (Hegde et al., 2008).

In summary, the work presented here reveals unusual structural features of Neil3 that provide an explanation for its preference for DNA with single-stranded regions. Neil3 not only lacks two of the three void-filling triad residues that serve an important function to stabilize the opposite strand in a duplex DNA, but it also harbors negatively charged residues on each side of the

damaged strand binding cleft, which would hinder binding of the opposite strand. Further, the loop corresponding to the 8-oxoG capping loop that caps 8-oxoG in bacterial Fpg proteins is truncated in Neil3. Therefore, it lacks the ability to stabilize the flipped-out 8-oxoG in the binding pocket. Neil3 glycosylases appear to protect mammalian cells from the mutagenic and/or cytotoxic effects of lesions in specialized ssDNA structures. Neil3 may also serve another yet unknown purpose in mammalian cells because it contains a ~30 kDa C-terminal extension of undetermined function.

EXPERIMENTAL PROCEDURES

Protein Expression and Purification

We have previously reported the cloning, expression, and purification of MmuNeil3Δ324 (Liu et al., 2012) (see details in the Supplemental Experimental Procedures).

Electrophoretic Mobility Shift Assay

EMSA assays were performed as described in the Supplemental Experimental Procedures.

Crystallization and Data Collection

MmuNeil3Δ324 crystals were obtained at 4°C with the hanging drop, vapor-diffusion method by mixing 1 μl of protein solution (12 mg/ml) in a 1:1 ratio with a reservoir solution containing 0.15 M DL-malic acid, 0.1 M HEPES-NaOH pH 7.0, 0.1 M NaI, and 18% (w/v) polyethylene glycol 3350 optimized from the Index HT screen followed by the use of an Additive screen (Hampton Research, Aliso Viejo, CA). Streak seeding was necessary to obtain well-diffracting crystals. Crystals were cryoprotected in a solution of mother liquor supplemented with 35% (v/v) glycerol, and flash-cooled into liquid nitrogen. The crystal belong to space group C2 with unit-cell dimensions a = 115.67 Å, b = 43.81 Å, c = 77.67 Å, and β = 128.94°, with one copy of MmuNeil3Δ324 per asymmetric unit. Diffraction data up to 2.1 Å resolution were collected at 100 K at a wavelength of 1.5418 Å on a MAR345 detector (MAR Research, Hamburg, Germany) mounted on a Rigaku RU200 rotating copper anode X-ray generator (Molecular Structure Corporation, The Woodlands, TX). A 2.0 Å anomalous scattering data set was collected at beamline 23-ID-B of the Advanced Photon Source (APS) at Argonne National Laboratory (Argonne, IL) at the zinc edge (wavelength of 1.2808 Å determined by X-ray fluorescence scan). Data sets were processed, scaled, and merged with Denzo/Scalepack (Otwinowski and Minor, 1997). Data collection statistics are summarized in Table 1.

Structure Determination and Refinement

Initial attempts to solve the phase problem by molecular replacement using the following models of enzymes of the Fpg/Nei family were unsuccessful: EcoFpg, Protein Data Bank (PDB) ID code 1K82 (Gilboa et al., 2002); EcoNei, PDB ID code 1K3W (Zharkov et al., 2002); TthFpg, PDB ID code 1EE8 (Sugahara et al., 2000); LlaFpg, PDB ID code 1TDZ (Coste et al., 2004); BstFpg, PDB ID code 1R2Y (Fromme and Verdine, 2003a); NEIL1, PDB ID code 1TDH (Doublié et al., 2004); and MvNei1, PDB ID code 3A46 (Imamura et al., 2009). The structure was therefore solved by multiple isomorphous replacement (MIR) using native and three derivative data sets—one gold potassium cyanide and two potassium tetrachloroplatinate (II). Crystals were soaked in 1 mM $KAu(CN)_2$ for 20 min, 0.1 mM K_2PtCl_4 for 6 hr, or 10 mM K_2PtCl_4 for 10 min (Joyce et al., 2010). The platinum sites in the two potassium tetrachloroplatinate (II) derivative sets were first located using difference Patterson maps generated by Fast Fourier Transform (FFT) in the CCP4 program suite (Read and Schierbeek, 1988). The initial phases, calculated using the platinum sites, were used to locate the gold sites by isomorphous difference Fourier methods. The heavy atom sites were then refined by SOLVE (Terwilliger and Berendzen, 1999). Although the best diffracting crystals were grown in the presence of iodide the halide ions did not contribute significantly to the electron density map and were therefore not included in the phasing process. An initial protein model was generated by RESOLVE (Terwilliger, 2004), and the rest of the model was built into the electron density map using Coot (Emsley and Cowtan, 2004). The position of the zinc atom was confirmed by an anomalous difference Fourier map. The final model was produced through iterative cycles of manual model building and refinement with CNS (Brunger, 2007), including simulated annealing, bulk solvent correction, grouped *B*-factor, and *B*-individual refinement. The free *R* factor was calculated with 10% of the reflections set aside. Two regions of the polypeptide chain, residues 37–59 and 113–116, had poorly defined or no electron density and were not built into the model. The final model comprises residues 2–36, 60–112, and 117–283 (including one histidine of the C-terminal 6-His tag). The quality of the model was evaluated with PROCHECK (Laskowski et al., 1993), and all nonglycine residues in the final model fall within the most favored or additionally allowed regions of the Ramachandran plot. Refinement statistics are shown in Table 1. All structure figures were prepared using the PyMOL Molecular Graphics System, Version 1.3, Schrödinger, LLC.

ACCESSION NUMBERS

The PDB accession number for the coordinates and structure factors of mouse Neil3 reported in this paper is 3W0F.

SUPPLEMENTAL INFORMATION

Supplemental Information includes fives figures and Supplemental Experimental Procedures and can be found with this article online at http://dx.doi.org/10.1016/j.str.2012.12.008.

ACKNOWLEDGMENTS

We would like to thank Dr. Cynthia J. Burrows, University of Utah, for providing oligodeoxyribonucleotides containing spiroiminodihydantoin, Dr. Pierre Aller and Karl Zahn for data collection at beamline 23-ID-B at the APS, and Drs. Qin Yang and Mark Rould for helpful crystallographic suggestions. This work was supported by National Institutes of Health Grant P01CA098993 awarded by the National Cancer Institute. The beamline GM/CA CAT has been funded in whole or in part by federal funds from the National Cancer Institute (Y1-CO-1020) and the National Institute of General Medical Science (Y1-GM-1104). Use of the APS was supported by the U.S. Department of Energy, Basic Energy Sciences, under contract no. DE-AC02-06CH11357.

Received: October 31, 2012
Revised: December 7, 2012
Accepted: December 8, 2012
Published: January 10, 2013

REFERENCES

Aller, P., Ye, Y., Wallace, S.S., Burrows, C.J., and Doublié, S. (2010). Crystal structure of a replicative DNA polymerase bound to the oxidized guanine lesion guanidinohydantoin. Biochemistry *49*, 2502–2509.

Bandaru, V., Sunkara, S., Wallace, S.S., and Bond, J.P. (2002). A novel human DNA glycosylase that removes oxidative DNA damage and is homologous to Escherichia coli endonuclease VIII. DNA Repair (Amst.) *1*, 517–529.

Bandaru, V., Zhao, X., Newton, M.R., Burrows, C.J., and Wallace, S.S. (2007). Human endonuclease VIII-like (NEIL) proteins in the giant DNA Mimivirus. DNA Repair (Amst.) *6*, 1629–1641.

Banerjee, A., Santos, W.L., and Verdine, G.L. (2006). Structure of a DNA glycosylase searching for lesions. Science *311*, 1153–1157.

Barrett, T.E., Savva, R., Panayotou, G., Barlow, T., Brown, T., Jiricny, J., and Pearl, L.H. (1998). Crystal structure of a G:T/U mismatch-specific DNA glycosylase: mismatch recognition by complementary-strand interactions. Cell *92*, 117–129.

Beckman, J., Wang, M., Blaha, G., Wang, J., and Konigsberg, W.H. (2010). Substitution of Ala for Tyr567 in RB69 DNA polymerase allows dAMP to be inserted opposite 7,8-dihydro-8-oxoguanine. Biochemistry *49*, 4116–4125.

Bruner, S.D., Norman, D.P., and Verdine, G.L. (2000). Structural basis for recognition and repair of the endogenous mutagen 8-oxoguanine in DNA. Nature *403*, 859–866.

Brunger, A.T. (2007). Version 1.2 of the Crystallography and NMR system. Nat. Protoc. *2*, 2728–2733.

Castaing, B., Boiteux, S., and Zelwer, C. (1992). DNA containing a chemically reduced apurinic site is a high affinity ligand for the E. coli formamidopyrimidine-DNA glycosylase. Nucleic Acids Res. *20*, 389–394.

Coste, F., Ober, M., Carell, T., Boiteux, S., Zelwer, C., and Castaing, B. (2004). Structural basis for the recognition of the FapydG lesion (2,6-diamino-4-hydroxy-5-formamidopyrimidine) by formamidopyrimidine-DNA glycosylase. J. Biol. Chem. *279*, 44074–44083.

David, S.S., O'Shea, V.L., and Kundu, S. (2007). Base-excision repair of oxidative DNA damage. Nature *447*, 941–950.

Dou, H., Mitra, S., and Hazra, T.K. (2003). Repair of oxidized bases in DNA bubble structures by human DNA glycosylases NEIL1 and NEIL2. J. Biol. Chem. *278*, 49679–49684.

Doublié, S., Bandaru, V., Bond, J.P., and Wallace, S.S. (2004). The crystal structure of human endonuclease VIII-like 1 (NEIL1) reveals a zincless finger motif required for glycosylase activity. Proc. Natl. Acad. Sci. USA *101*, 10284–10289.

Duclos, S., Doublié, S., and Wallace, S.S. (2012a). Consequences and Repair of Oxidative DNA Damage (London, UK: Royal Society of Chemistry), pp. 109–153.

Duclos, S., Aller, P., Jaruga, P., Dizdaroglu, M., Wallace, S.S., and Doublié, S. (2012b). Structural and biochemical studies of a plant formamidopyrimidine-DNA glycosylase reveal why eukaryotic Fpg glycosylases do not excise 8-oxoguanine. DNA Repair (Amst.) *11*, 714–725.

Dunn, A.R., Kad, N.M., Nelson, S.R., Warshaw, D.M., and Wallace, S.S. (2011). Single Qdot-labeled glycosylase molecules use a wedge amino acid to probe for lesions while scanning along DNA. Nucleic Acids Res. *39*, 7487–7498.

Emsley, P., and Cowtan, K. (2004). Coot: model-building tools for molecular graphics. Acta Crystallogr. D Biol. Crystallogr. *60*, 2126–2132.

Fromme, J.C., and Verdine, G.L. (2002). Structural insights into lesion recognition and repair by the bacterial 8-oxoguanine DNA glycosylase MutM. Nat. Struct. Biol. *9*, 544–552.

Fromme, J.C., and Verdine, G.L. (2003a). DNA lesion recognition by the bacterial repair enzyme MutM. J. Biol. Chem. *278*, 51543–51548.

Fromme, J.C., and Verdine, G.L. (2003b). Structure of a trapped endonuclease III-DNA covalent intermediate. EMBO J. *22*, 3461–3471.

Fromme, J.C., Banerjee, A., Huang, S.J., and Verdine, G.L. (2004). Structural basis for removal of adenine mispaired with 8-oxoguanine by MutY adenine DNA glycosylase. Nature *427*, 652–656.

Gilboa, R., Zharkov, D.O., Golan, G., Fernandes, A.S., Gerchman, S.E., Matz, E., Kycia, J.H., Grollman, A.P., and Shoham, G. (2002). Structure of formamidopyrimidine-DNA glycosylase covalently complexed to DNA. J. Biol. Chem. *277*, 19811–19816.

Golan, G., Zharkov, D.O., Feinberg, H., Fernandes, A.S., Zaika, E.I., Kycia, J.H., Grollman, A.P., and Shoham, G. (2005). Structure of the uncomplexed DNA repair enzyme endonuclease VIII indicates significant interdomain flexibility. Nucleic Acids Res. *33*, 5006–5016.

Hashimoto, H., Zhang, X., and Cheng, X. (2012). Excision of thymine and 5-hydroxymethyluracil by the MBD4 DNA glycosylase domain: structural basis and implications for active DNA demethylation. Nucleic Acids Res. *40*, 8276–8284.

Haushalter, K.A., Todd Stukenberg, M.W., Kirschner, M.W., and Verdine, G.L. (1999). Identification of a new uracil-DNA glycosylase family by expression cloning using synthetic inhibitors. Curr. Biol. *9*, 174–185.

Hazra, T.K., Izumi, T., Boldogh, I., Imhoff, B., Kow, Y.W., Jaruga, P., Dizdaroglu, M., and Mitra, S. (2002a). Identification and characterization of a human DNA glycosylase for repair of modified bases in oxidatively damaged DNA. Proc. Natl. Acad. Sci. USA *99*, 3523–3528.

Hazra, T.K., Kow, Y.W., Hatahet, Z., Imhoff, B., Boldogh, I., Mokkapati, S.K., Mitra, S., and Izumi, T. (2002b). Identification and characterization of a novel human DNA glycosylase for repair of cytosine-derived lesions. J. Biol. Chem. *277*, 30417–30420.

Hegde, M.L., Hazra, T.K., and Mitra, S. (2008). Early steps in the DNA base excision/single-strand interruption repair pathway in mammalian cells. Cell Res. *18*, 27–47.

Hildrestrand, G.A., Neurauter, C.G., Diep, D.B., Castellanos, C.G., Krauss, S., Bjørås, M., and Luna, L. (2009). Expression patterns of Neil3 during embryonic brain development and neoplasia. BMC Neurosci. *10*, 45.

Imamura, K., Wallace, S.S., and Doublié, S. (2009). Structural characterization of a viral NEIL1 ortholog unliganded and bound to abasic site-containing DNA. J. Biol. Chem. *284*, 26174–26183.

Imamura, K., Averill, A., Wallace, S.S., and Doublié, S. (2012). Structural characterization of viral ortholog of human DNA glycosylase NEIL1 bound to thymine glycol or 5-hydroxyuracil-containing DNA. J. Biol. Chem. *287*, 4288–4298.

Ishchenko, A.A., Bulychev, N.V., Maksakova, G.A., Johnson, F., and Nevinsky, G.A. (1999). Single-stranded oligodeoxyribonucleotides are substrates of Fpg protein from Escherichia coli. IUBMB Life *48*, 613–618.

Jia, L., Shafirovich, V., Shapiro, R., Geacintov, N.E., and Broyde, S. (2005). Structural and thermodynamic features of spiroiminodihydantoin damaged DNA duplexes. Biochemistry *44*, 13342–13353.

Joyce, M.G., Radaev, S., and Sun, P.D. (2010). A rational approach to heavy-atom derivative screening. Acta Crystallogr. D Biol. Crystallogr. *66*, 358–365.

Kabsch, W., and Sander, C. (1983). Dictionary of protein secondary structure: pattern recognition of hydrogen-bonded and geometrical features. Biopolymers *22*, 2577–2637.

Kathe, S.D., Barrantes-Reynolds, R., Jaruga, P., Newton, M.R., Burrows, C.J., Bandaru, V., Dizdaroglu, M., Bond, J.P., and Wallace, S.S. (2009). Plant and fungal Fpg homologs are formamidopyrimidine DNA glycosylases but not 8-oxoguanine DNA glycosylases. DNA Repair (Amst.) *8*, 643–653.

Kauffmann, A., Rosselli, F., Lazar, V., Winnepenninckx, V., Mansuet-Lupo, A., Dessen, P., van den Oord, J.J., Spatz, A., and Sarasin, A. (2008). High expression of DNA repair pathways is associated with metastasis in melanoma patients. Oncogene *27*, 565–573.

Kavli, B., Sundheim, O., Akbari, M., Otterlei, M., Nilsen, H., Skorpen, F., Aas, P.A., Hagen, L., Krokan, H.E., and Slupphaug, G. (2002). hUNG2 is the major repair enzyme for removal of uracil from U:A matches, U:G mismatches, and U in single-stranded DNA, with hSMUG1 as a broad specificity backup. J. Biol. Chem. *277*, 39926–39936.

Kornyushyna, O., Berges, A.M., Muller, J.G., and Burrows, C.J. (2002). In vitro nucleotide misinsertion opposite the oxidized guanosine lesions spiroiminodihydantoin and guanidinohydantoin and DNA synthesis past the lesions using Escherichia coli DNA polymerase I (Klenow fragment). Biochemistry *41*, 15304–15314.

Krissinel, E., and Henrick, K. (2004). Secondary-structure matching (SSM), a new tool for fast protein structure alignment in three dimensions. Acta Crystallogr. D Biol. Crystallogr. *60*, 2256–2268.

Krokeide, S.Z., Bolstad, N., Laerdahl, J.K., Bjørås, M., and Luna, L. (2009). Expression and purification of NEIL3, a human DNA glycosylase homolog. Protein Expr. Purif. *65*, 160–164.

Kropachev, K.Y., Zharkov, D.O., and Grollman, A.P. (2006). Catalytic mechanism of Escherichia coli endonuclease VIII: roles of the intercalation loop and the zinc finger. Biochemistry *45*, 12039–12049.

Laskowski, R.A., MacArthur, M.W., Moss, D.S., and Thornton, J.M. (1993). PROCHECK: a program to check the stereochemical quality of protein structures. J. Appl. Cryst. *26*, 283–291.

Lau, A.Y., Schärer, O.D., Samson, L., Verdine, G.L., and Ellenberger, T. (1998). Crystal structure of a human alkylbase-DNA repair enzyme complexed to DNA: mechanisms for nucleotide flipping and base excision. Cell *95*, 249–258.

Liu, M., Bandaru, V., Bond, J.P., Jaruga, P., Zhao, X., Christov, P.P., Burrows, C.J., Rizzo, C.J., Dizdaroglu, M., and Wallace, S.S. (2010). The mouse ortholog of NEIL3 is a functional DNA glycosylase in vitro and in vivo. Proc. Natl. Acad. Sci. USA *107*, 4925–4930.

Liu, M., Bandaru, V., Holmes, A., Averill, A.M., Cannan, W., and Wallace, S.S. (2012). Expression and purification of active mouse and human NEIL3 proteins. Protein Expr. Purif. *84*, 130–139.

Maiti, A., Morgan, M.T., Pozharski, E., and Drohat, A.C. (2008). Crystal structure of human thymine DNA glycosylase bound to DNA elucidates sequence-specific mismatch recognition. Proc. Natl. Acad. Sci. USA *105*, 8890–8895.

Manvilla, B.A., Maiti, A., Begley, M.C., Toth, E.A., and Drohat, A.C. (2012). Crystal structure of human methyl-binding domain IV glycosylase bound to abasic DNA. J. Mol. Biol. *420*, 164–175.

Mol, C.D., Arvai, A.S., Slupphaug, G., Kavli, B., Alseth, I., Krokan, H.E., and Tainer, J.A. (1995). Crystal structure and mutational analysis of human uracil-DNA glycosylase: structural basis for specificity and catalysis. Cell *80*, 869–878.

Morland, I., Rolseth, V., Luna, L., Rognes, T., Bjørås, M., and Seeberg, E. (2002). Human DNA glycosylases of the bacterial Fpg/MutM superfamily: an alternative pathway for the repair of 8-oxoguanine and other oxidation products in DNA. Nucleic Acids Res. *30*, 4926–4936.

Neurauter, C.G., Luna, L., and Bjørås, M. (2012). Release from quiescence stimulates the expression of human NEIL3 under the control of the Ras dependent ERK-MAP kinase pathway. DNA Repair (Amst.) *11*, 401–409.

Nicholls, A., Sharp, K.A., and Honig, B. (1991). Protein folding and association: insights from the interfacial and thermodynamic properties of hydrocarbons. Proteins *11*, 281–296.

Otwinowski, Z., and Minor, W. (1997). Processing of X-ray Diffraction Data Collected in Oscillation Mode (New York: Academic Press), pp. 307–326.

Parikh, S.S., Mol, C.D., Slupphaug, G., Bharati, S., Krokan, H.E., and Tainer, J.A. (1998). Base excision repair initiation revealed by crystal structures and binding kinetics of human uracil-DNA glycosylase with DNA. EMBO J. *17*, 5214–5226.

Prakash, A., Doublié, S., and Wallace, S.S. (2012). The Fpg/Nei family of DNA glycosylases: substrates, structures, and search for damage. Prog. Mol. Biol. Transl. Sci. *110*, 71–91.

Read, R.J., and Schierbeek, A.J. (1988). A phased translation function. J. Appl. Crystallogr. *21*, 490–495.

Regnell, C.E., Hildrestrand, G.A., Sejersted, Y., Medin, T., Moldestad, O., Rolseth, V., Krokeide, S.Z., Suganthan, R., Luna, L., Bjørås, M., and Bergersen, L.H. (2012). Hippocampal adult neurogenesis is maintained by Neil3-dependent repair of oxidative DNA lesions in neural progenitor cells. Cell Rep. *2*, 503–510.

Rolseth, V., Rundén-Pran, E., Luna, L., McMurray, C., Bjørås, M., and Ottersen, O.P. (2008). Widespread distribution of DNA glycosylases removing oxidative DNA lesions in human and rodent brains. DNA Repair (Amst.) *7*, 1578–1588.

Savva, R., McAuley-Hecht, K., Brown, T., and Pearl, L. (1995). The structural basis of specific base-excision repair by uracil-DNA glycosylase. Nature *373*, 487–493.

Sejersted, Y., Hildrestrand, G.A., Kunke, D., Rolseth, V., Krokeide, S.Z., Neurauter, C.G., Suganthan, R., Atneosen-Åsegg, M., Fleming, A.M., Saugstad, O.D., et al. (2011). Endonuclease VIII-like 3 (Neil3) DNA glycosylase promotes neurogenesis induced by hypoxia-ischemia. Proc. Natl. Acad. Sci. USA *108*, 18802–18807.

Serre, L., Pereira de Jésus, K., Boiteux, S., Zelwer, C., and Castaing, B. (2002). Crystal structure of the Lactococcus lactis formamidopyrimidine-DNA glycosylase bound to an abasic site analogue-containing DNA. EMBO J. *21*, 2854–2865.

Sidorenko, V.S., and Zharkov, D.O. (2008). Correlated cleavage of damaged DNA by bacterial and human 8-oxoguanine-DNA glycosylases. Biochemistry *47*, 8970–8976.

Slupphaug, G., Mol, C.D., Kavli, B., Arvai, A.S., Krokan, H.E., and Tainer, J.A. (1996). A nucleotide-flipping mechanism from the structure of human uracil-DNA glycosylase bound to DNA. Nature *384*, 87–92.

Sugahara, M., Mikawa, T., Kumasaka, T., Yamamoto, M., Kato, R., Fukuyama, K., Inoue, Y., and Kuramitsu, S. (2000). Crystal structure of a repair enzyme of oxidatively damaged DNA, MutM (Fpg), from an extreme thermophile, Thermus thermophilus HB8. EMBO J. *19*, 3857–3869.

Takao, M., Kanno, S., Kobayashi, K., Zhang, Q.M., Yonei, S., van der Horst, G.T., and Yasui, A. (2002). A back-up glycosylase in Nth1 knock-out mice is a functional Nei (endonuclease VIII) homologue. J. Biol. Chem. *277*, 42205–42213.

Takao, M., Oohata, Y., Kitadokoro, K., Kobayashi, K., Iwai, S., Yasui, A., Yonei, S., and Zhang, Q.M. (2009). Human Nei-like protein NEIL3 has AP lyase activity specific for single-stranded DNA and confers oxidative stress resistance in Escherichia coli mutant. Genes Cells *14*, 261–270.

Terwilliger, T. (2004). SOLVE and RESOLVE: automated structure solution, density modification and model building. J. Synchrotron Radiat. *11*, 49–52.

Terwilliger, T.C., and Berendzen, J. (1999). Automated MAD and MIR structure solution. Acta Crystallogr. D Biol. Crystallogr. *55*, 849–861.

Torisu, K., Tsuchimoto, D., Ohnishi, Y., and Nakabeppu, Y. (2005). Hematopoietic tissue-specific expression of mouse Neil3 for endonuclease VIII-like protein. J. Biochem. *138*, 763–772.

Wallace, S.S. (2002). Biological consequences of free radical-damaged DNA bases. Free Radic. Biol. Med. *33*, 1–14.

Wallace, S.S., Bandaru, V., Kathe, S.D., and Bond, J.P. (2003). The enigma of endonuclease VIII. DNA Repair (Amst.) *2*, 441–453.

Wibley, J.E., Waters, T.R., Haushalter, K., Verdine, G.L., and Pearl, L.H. (2003). Structure and specificity of the vertebrate anti-mutator uracil-DNA glycosylase SMUG1. Mol. Cell *11*, 1647–1659.

Xiao, G., Tordova, M., Jagadeesh, J., Drohat, A.C., Stivers, J.T., and Gilliland, G.L. (1999). Crystal structure of Escherichia coli uracil DNA glycosylase and its complexes with uracil and glycerol: structure and glycosylase mechanism revisited. Proteins *35*, 13–24.

Zhao, X., Krishnamurthy, N., Burrows, C.J., and David, S.S. (2010). Mutation versus repair: NEIL1 removal of hydantoin lesions in single-stranded, bulge, bubble, and duplex DNA contexts. Biochemistry *49*, 1658–1666.

Zharkov, D.O., Shoham, G., and Grollman, A.P. (2003). Structural characterization of the Fpg family of DNA glycosylases. DNA Repair (Amst.) *2*, 839–862.

Zharkov, D.O., Golan, G., Gilboa, R., Fernandes, A.S., Gerchman, S.E., Kycia, J.H., Rieger, R.A., Grollman, A.P., and Shoham, G. (2002). Structural analysis of an Escherichia coli endonuclease VIII covalent reaction intermediate. EMBO J. *21*, 789–800.

